Advanced Antibacterial Materials
https://www.sciltp.com/journals/aam

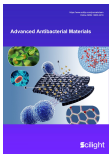

Article

Titanium Implant Functionalized with D-Amino Acid-Substituted Antimicrobial Peptides for Infection Resistance and Enhanced Biocompatibility

Ru Zhong [1,2,3], Lin Wang [1,2,3,*] and Yingjun Wang [1,2,3,*]

[1] National Engineering Research Center for Tissue Restoration and Reconstruction, South China University of Technology, Guangzhou 510006, China
[2] School of Material Science and Engineering, South China University of Technology, Guangzhou 510006, China
[3] Guangdong Provincial Key Laboratory of Biomedical Engineering, South China University of Technology, Guangzhou 510006, China
* Correspondence: wanglin3@scut.edu.cn (L.W.); imwangyj@scut.edu.cn (Y.W.)

How To Cite: Zhong, R.; Wang, L.; Wang, Y. Titanium Implant Functionalized with D-Amino Acid-Substituted Antimicrobial Peptides for Infection Resistance and Enhanced Biocompatibility. *Advanced Antibacterial Materials* **2026**, *1*(1), 78–87. https://doi.org/10.53941/aam.2026.100006

Received: 22 December 2025
Revised: 15 January 2026
Accepted: 16 January 2026
Published: 3 February 2026

Abstract: Antimicrobial peptide (AMP) coatings show potential in preventing implant-associated infections (IAI), but their effectiveness is frequently limited by enzymatic degradation and cytotoxicity at elevated densities. This study demonstrates that complete D-amino acid substitution of surface-grafted AMPs effectively addresses these shortcomings. Using a model antimicrobial peptide (DRAMP04195) covalently immobilized on titanium via strain-promoted azide-alkyne cycloaddition (SPAAC), we compared the L- and D-peptide variants. At a high grafting density, Ti-D-80 achieves near-complete eradication of both *S. aureus* and *E. coli* (>99.99%), outperforming Ti-L-80. Scanning electron microscopy confirms membrane disruption as the primary antibacterial mechanism for both surfaces. Importantly, Ti-D-80 retains over 90% of its antibacterial activity after protease treatment, whereas Ti-L-80 is almost completely inactivated. Moreover, Ti-D-80 exhibits excellent biocompatibility, supporting cell adhesion and proliferation comparable to that of pristine titanium, in contrast to the cytotoxicity observed with Ti-L-80. These findings establish D-amino acid substitution as an effective strategy to simultaneously enhance enzymatic stability, antibacterial potency, and biocompatibility of AMP-functionalized implants, providing a robust approach for designing durable and tissue-compatible antimicrobial interfaces.

Keywords: antimicrobial peptides; D-amino acid substitution; titanium implant; surface grafting; biocompatibility

1. Introduction

Titanium implants are extensively employed in orthopedic and dental implants owing to their favorable mechanical properties, corrosion resistance, and biocompatibility [1]. However, their inherent bio-inert nature renders the surfaces prone to bacterial colonization, which can lead to implant-associated infections (IAIs), a significant clinical complication [2,3]. Upon adhesion to the implant surface, pathogenic bacteria secrete extracellular polymeric substances that facilitate biofilm formation [4]. These biofilms act as a protective barrier, hindering antibiotic penetration and leading to persistent infections that are resistant to both host immune defenses and conventional antimicrobial therapies [5]. Managing such infections often requires revision surgeries, imposing substantial economic burdens on healthcare systems [6,7].

Current preventive measures against IAIs predominantly rely on systemic or localized antibiotic delivery [8]. However, the rising prevalence of multidrug-resistant bacteria, combined with the short half-life and potential

systemic toxicity of many antibiotics, has markedly limited their long-term efficacy [9,10]. Alternative antibacterial coating strategies, such as those based on metallic ions [11,12] or antibiotics [13–15], are frequently hampered by issues like cytotoxic side effects. Consequently, there is an urgent need to develop surface modification approaches that can confer durable, stable, and non-resistance-inducing antibacterial properties to titanium implants.

Antimicrobial peptides (AMPs) have attracted considerable interest as next-generation therapeutic agents due to their unique structural features and distinct mechanisms of action against pathogens [16]. Their capacity to disrupt microbial membranes and target intracellular components, while minimizing the risk of inducing bacterial resistance, makes them particularly appealing for biomedical applications [17,18]. In recent years, immobilizing AMPs onto titanium surfaces to create localized antibacterial interfaces has been widely explored [19–22]. However, most natural and synthetic AMPs are composed of L-amino acids, which are susceptible to degradation by host and bacterial proteases in physiological environments. However, most natural and synthetic AMPs are composed of L-amino acids, which are susceptible to degradation by host and bacterial proteases in physiological environments [23,24].

To address this limitation, the strategy of constructing all-D-amino acid-substituted AMPs has emerged as a promising solution. Owing to the chiral specificity of proteases, which preferentially cleave L-peptide bonds, D-AMPs—with their inverted stereo configuration—exhibit remarkable resistance to enzymatic hydrolysis and demonstrate superior proteolytic stability [23–25]. Solution-phase studies have confirmed that D-AMPs maintain potent antibacterial activity in the presence of proteases or serum, whereas their L-counterparts are rapidly inactivated [23]. This provides a strong rationale for their application in biomedical surface engineering. While recent studies have successfully grafted D-AMPs onto aluminum surfaces and demonstrated their antibacterial activity [26], critical questions remain unresolved regarding both the comparative efficacy of equally dense L- and D-AMP coatings and the retention of enzymatic stability after surface immobilization. Furthermore, the differential effects of D-AMP- and L-AMP-modified surfaces on cellular adhesion and proliferation have not been investigated. Addressing these specific gaps is essential to advance D-AMP-based coatings toward clinical translation.

In this study, we selected a model peptide (DRAMP04195, sequence Lys-Lys-Leu-Leu-Lys-Lys-Leu-Leu-Lys-Trp-Leu) with documented antibacterial activity from the DRAMP database [27,28]. The peptide was functionalized with an N_3–PEG_{12} linker at its N-terminus, while the titanium surface was grafted with DBCO-silane. Covalent immobilization was achieved via strain-promoted azide-alkyne cycloaddition (SPAAC). By comparing the antibacterial performance, enzymatic stability, and biocompatibility of surfaces grafted with the D-substituted peptide and its native L-form, this work aimed to provide evidence for developing robust surface functionalization strategies based on D-amino acid-substituted antimicrobial peptides.

2. Materials and Methods

2.1. Materials

Pure titanium (Ti) sheets were supplied by Hebei Shengyuan Metal Co., Ltd. (Cangzhou, China). Sodium hydroxide (NaOH) was purchased from Guangzhou Chemical Reagent Factory (Guangzhou, China). The silane coupling agent modified with DBCO-$PEG_{3.4k}$ (DBCO-sil) was sourced from Posure Biotechnology (Shanghai, China). Peptides were synthesized and provided by QYAOBIO (Shanghai, China). The Micro-BCA protein assay kit was obtained from Thermo Fisher Scientific (Rockford, IL, USA). The bacteria *Staphylococcus aureus* (*S. aureus*, ATCC 6538p) and *Escherichia coli* (*E. coli*, ATCC 8739) were obtained from the Guangdong Microbial Culture Collection Center (GDMCC). The L929 cell line was sourced from Procell Life Science & Technology Co., Ltd. (Wuhan, China). Proteinase K was purchased from Macklin Inc. (Shanghai, China). The CCK-8 reagent was obtained from Dojindo Laboratories (Kumamoto, Japan). The cytoskeletal staining dye FITC-labeled phalloidin was acquired from AAT Bioquest (Pleasanton, CA, USA), and DAPI was obtained from Beyotime Biotechnology (Nantong, China).

2.2. Surface Grafting

Pure titanium sheets (1 × 1 cm^2) were ultrasonically cleaned sequentially in anhydrous ethanol and water for 5 min each, then dried with N_2. The titanium sheets were immersed in 1 mL of 5M NaOH solution and subjected to alkali treatment at 60 °C for 24 h. Subsequently, the sheets were ultrasonically cleaned with deionized water twice, for 2 min each time. Then, 0.5 mg/mL DBCO-$PEG_{3.4k}$-Silane (in 95% ethanol) was added for grafting at room temperature for 24 h, followed by curing at 100 °C for 30 min. After washing with deionized water and drying with N_2, the silanized samples (Ti-S) were obtained. Peptide solutions at different concentrations were prepared using deionized water. The samples were immersed in the peptide solutions for grafting at room temperature for 6 h, then ultrasonically cleaned and dried with N_2 to obtain the peptide-grafted samples. The

following peptide sequences were used: L-peptide, with the sequence N_3-PEG_{12}-KKLLKKLLKWL (designated as L), and its D-amino acid substituted counterpart, N_3-PEG_{12}-kkllkkllkwl (designated as D). The corresponding grafted surfaces were designated as Ti-L and Ti-D, with the suffix (-X) indicating the grafting concentration (μM).

2.3. Peptide Quantification

Peptide density on the surface was quantified using a Micro-BCA kit (Thermo Fisher Scientific, Rockford, IL, USA). The working solution was prepared with a ratio of MA:MB:MC = 25:24:1. The reaction system consisted of 150 μL of sample and 150 μL of BCA working solution, which was sealed and incubated in a constant temperature shaker at 37 °C and 85 rpm for 2 h. The standard curve was established using peptide solutions ranging from 3.75 to 120 μM. Deionized water was used as the sample solution for surface quantification. The surface peptide grafting amount was calculated based on the peptide concentration-OD value standard curve. The surface grafting density was determined using the following procedure. (1) The peptide-specific signal correction: $OD_{Peptide} = OD_{Sample} - OD_{Ti\text{-}S}$. All measured OD values, including both the standard curve and the samples, were first corrected by subtracting OD_{Blank} (a mixture of aqueous solution and Micro-BCA working reagent). (2) Concentration conversion: The corrected OD value was then converted to the corresponding peptide concentration (C, in μM) using the established standard curves. (3) Peptide density calculation: Peptide density (molecules/nm^2) = ($N_a \times C \times V$)/S, where N_a is Avogadro's constant (6.022×10^{23} /mol), V is the peptide solution volume (150 μL), and S is the surface area of the substrate (1 cm^2).

2.4. Antibacterial Activity in Solution

Peptide solutions and bacteria (*S. aureus* ATCC6538p and *E. coli* ATCC8739) were co-incubated in PBS (pH 7.4), with final peptide concentrations of 0, 2, 5, 10, 15, 20, 25, and 30 μM, and a bacterial concentration of 10^6 CFU/mL. After incubation for 2 h, the mixtures were serially diluted and plated for colony counting. The specific definitions and calculations are as follows: Bacterial viability (%) = ($CFU_{Sample}/CFU_{Control}$) × 100%, Antibacterial rate (%) = 100% − Bacterial viability (%), where the Control group refers to the condition where no peptide was added (0 μM).

2.5. Antibacterial Activity of Surfaces

S. aureus (ATCC6538p) and *E. coli* (ATCC8739) were diluted with PBS to obtain bacterial suspensions at 10^6 CFU/mL. 10 μL of the bacterial suspension was dropped on the samples and incubated for 2 h. After serial dilution with PBS, the solutions were spread onto agar plates for colony counting. The antibacterial rate was determined as described previously, with the Ti group serving as the Control.

2.6. Enzymatic Resistance

Proteinase K (100 μg/mL) was prepared in PBS (pH 7.4) and co-incubated with the samples for 30 min. The samples were then washed twice with PBS, inactivated at 95 °C for 30 min, ultrasonically cleaned with deionized water for 2 min, and dried with N_2. The surface antibacterial activity test was then performed as described above.

2.7. Bacterial Morphology

10 μL of bacterial suspensions (10^7 CFU/mL, *S. aureus* and *E. coli*) were dropped onto the sample surfaces and incubated for 2 h. The samples were fixed with 2.5% glutaraldehyde, followed by gradient dehydration with anhydrous ethanol. Finally, tert-butanol was added, and the samples were freeze-dried. After sputter-coating with gold for 60 s, the samples were observed by scanning electron microscope (SEM, Merlin, Zeiss, Germany) at a magnification of 20,000×.

2.8. Biocompatibility

Samples (1 × 1 cm^2) were placed in 24-well plates and sterilized overnight under UV light. After moistening the samples with DMEM culture medium (10%FBS), L929 cells were seeded at 10^4 cells per well and co-cultivated (37 °C, 5% CO_2) for 1, 3, and 5 days, with the medium changed on day 3. The samples were then transferred to a new 24-well plate. A CCK-8 working solution was prepared by mixing CCK-8 reagent and culture medium at a 1:10 ratio. 300 μL of the working solution was added to each well, and the plates were incubated in the cell culture incubator for 2 h. Then, 100 μL of the culture medium from each well was taken to measure the OD value at 450 nm.

2.9. Cytoskeleton Staining

Following the same procedure described above, cells were seeded on the samples. Samples co-cultured with L929 for 1, 3, and 5 days were fixed with 4% paraformaldehyde, permeabilized with Triton X-100 for 8 min, stained with Phalloidin-FITC solution for 1 h, and then stained with DAPI for 8 min. PBS washes were performed between each step. Cell morphology was observed and imaged using a fluorescence microscope (DM6M, Leica, Germany) with 420/488 nm filters.

2.10. Statistical Analysis

Data were presented as mean ± SD (n ≥ 3). Statistical significance was determined by two-tailed Student's *t*-test using Excel and Origin 8.0.2 software, and was defined as follows: * denoted $p < 0.05$, ** denoted $p < 0.01$, *** denoted $p < 0.001$; NS indicates not significant.

3. Results

3.1. Preparation and Characterization of Peptide Functionalized Titanium Surfaces

First, L- and D-peptides were covalently immobilized onto titanium substrates via strain-promoted azide-alkyne cycloaddition (SPAAC), generating Ti-L and Ti-D surfaces, respectively (Figure 1a). Then, the surface peptide density was quantified using a Micro BCA assay. Calibration curves for both peptides showed nearly identical slopes with excellent linear correlation ($R^2 > 0.98$, Figure 1b). Over the tested concentration range of 10 to 80 μM, the grafted peptide density increased proportionally with concentration (Figure 1c). At the highest concentration of 80 μM, the Ti-L and Ti-D surfaces exhibited comparable grafting densities of 28.13 ± 2.55 molecules/nm^2 (9.52 μg/cm^2) and 27.70 ± 1.30 molecules/nm^2 (9.37 μg/cm^2), respectively (Figure 1c).

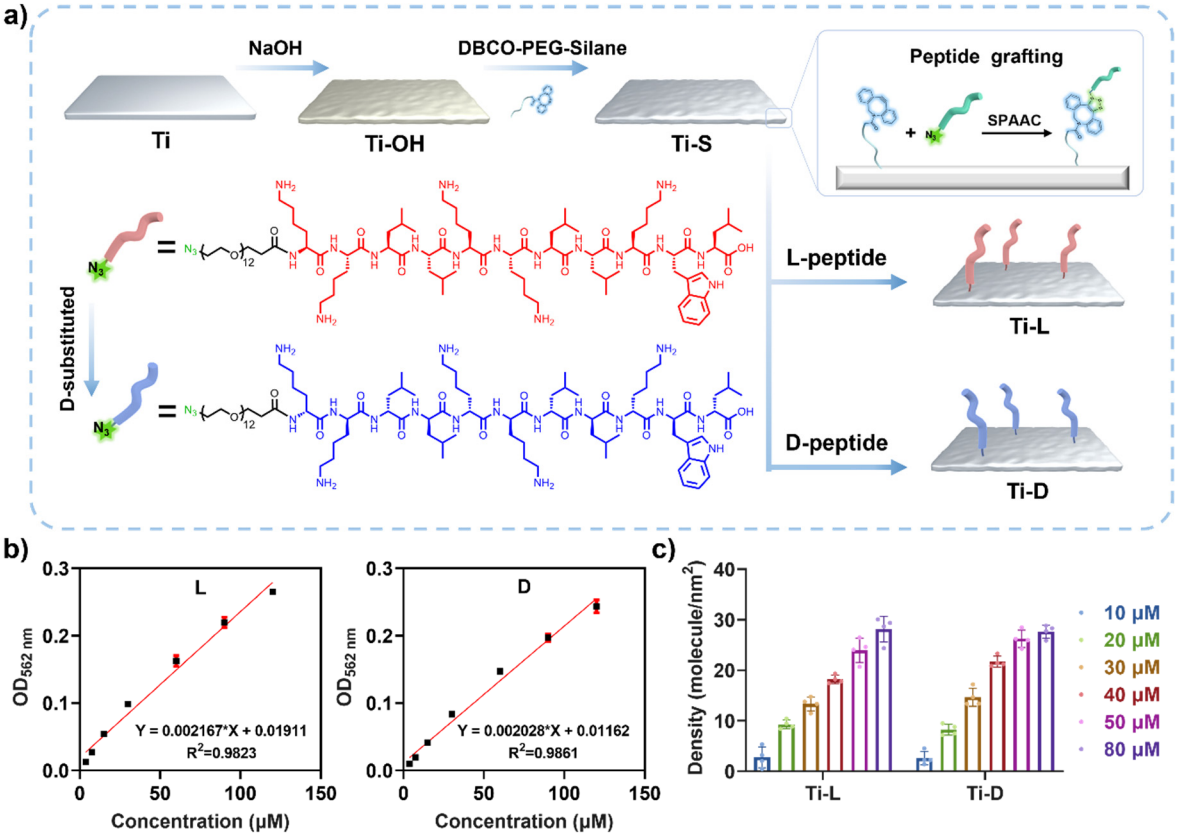

Figure 1. Preparation and characterization of peptide functionalized titanium surfaces. (**a**) Schematic illustration of surface functionalization via strain-promoted azide-alkyne cycloaddition (SPAAC). (**b**) Micro-BCA calibration curves for L- and D-peptides (n = 4). (**c**) Quantified peptide grafting densities on surfaces prepared at varying peptide concentrations (n = 4).

3.2. Antibacterial Activity of the Peptide Functionalized Titanium Surfaces

The antibacterial activity of the L-peptide and its all-D-amino acid substituted analogue (D-peptide) was evaluated in solution against Gram-positive *S. aureus* and Gram-negative *E. coli* to determine the effect of chiral inversion. As depicted in Figure 2a, a concentration-dependent increase in antibacterial rate was observed for both peptides. Comparative analysis revealed that the D-peptide possessed markedly enhanced potency. Against *S. aureus*, a 99.99% bactericidal rate was attained by the L-peptide at 25 μM, whereas the D-peptide achieved the same efficacy at 15 μM. In the case of *E. coli*, the L-peptide inhibited 96.21% of bacterial growth at 30 μM. In contrast, the D-peptide demonstrated 97.73% inhibition at 15 μM and complete (99.99%) inhibition at 30 μM. These findings indicated that complete D-amino acid substitution substantially increased the antibacterial potency of the peptide, enabling broad-spectrum pathogen eradication at reduced concentrations.

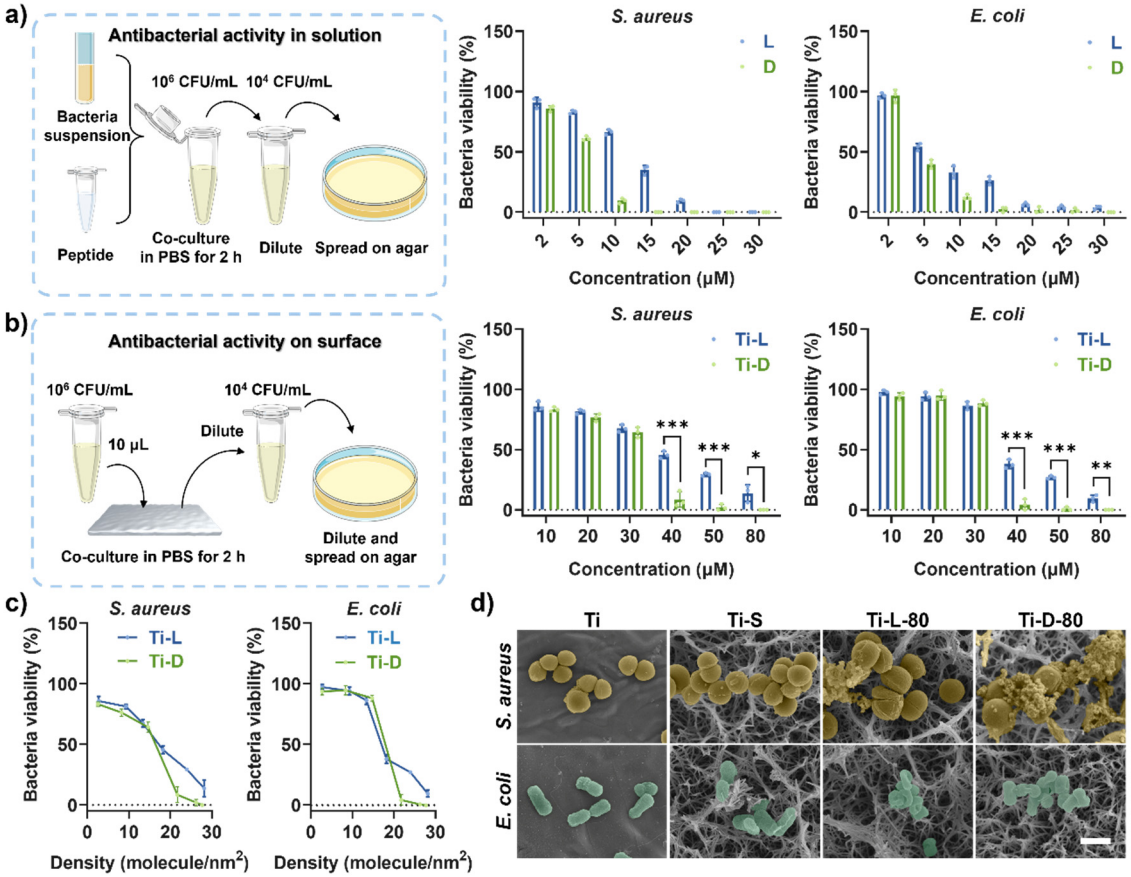

Figure 2. Antibacterial Activity of peptide functionalized titanium surfaces. (**a**) Dose-dependent antibacterial activity of L- and D-peptides in solution against *S. aureus* and *E. coli* (n = 3). (**b**) Antibacterial activity of surfaces functionalized at different peptide reaction concentrations against *S. aureus* and *E. coli* (n = 3). (**c**) Antibacterial activity of surfaces with varying peptide grafting densities against *S. aureus* and *E. coli* (n = 3). (**d**) SEM morphology of *S. aureus* and *E. coli* following incubation on indicated surfaces (scale bar = 1 μm). * Denoted $p < 0.05$, ** denoted $p < 0.01$, *** denoted $p < 0.001$.

Antibacterial assessment across surfaces with varying peptide reaction concentration revealed a clear dose-dependent enhancement in bactericidal activity. At the highest peptide reaction concentration (80 μM), Ti-L surfaces achieved 86.18% inhibition against *S. aureus* and 90.59% against *E. coli*, whereas Ti-D surfaces showed near-complete eradication (>99.99%) against both strains (Figure 2b). The correlation between peptide grafted density and antibacterial activity (Figure 2c) further confirmed that higher peptide loading consistently strengthened bactericidal effects. Notably, at comparable surface densities (>20 molecules/nm^2), Ti-D surfaces exhibited significantly superior antibacterial performance relative to Ti-L, consistent with trends observed in solution. These results demonstrated that the D-peptide retained higher antibacterial activity than its L-counterpart even after surface immobilization, and that the SPAAC-based grafting strategy effectively preserved the bioactive function of the peptides.

Furthermore, scanning electron microscopy (SEM) was employed to investigate the morphological alterations in *S. aureus* and *E. coli* following co-incubation with the substrates (Figure 2d). Bacteria grown on control surfaces of Ti and Ti-S exhibited typical and healthy growth characteristics. *S. aureus* appeared as smooth, spherical cells, whereas *E. coli* displayed a regular rod-shaped morphology. These bacteria were plump, uniform in size, and showed signs of normal binary fission, indicating active log-phase growth and confirming that the surfaces had no inherent growth-inhibitory or toxic effects. In contrast, on Ti-L-80 and Ti-D-80 surfaces, both bacterial species showed clear evidence of membrane stress and damage. Compared with the controls, *S. aureus* lost its rigid cell wall architecture and underwent irregular shrinkage accompanied by leakage of intracellular contents. More notably, *E. coli* exhibited marked morphological alterations, including significantly reduced cell length and the appearance of a characteristic central constriction that transformed the rods into a disk-like shape. This morphology strongly suggests a surface-mediated membrane damage mechanism [29]. Following disruption of membrane integrity by the antimicrobial peptides, efflux of cytoplasmic components combined with influx of external medium likely caused collapse of the cell envelope due to loss of turgor pressure. Collectively, these observations demonstrated that the primary antibacterial mechanism of both Ti-L and Ti-D surfaces operated through the disruption of bacterial membrane integrity.

3.3. Enzymatic Stability of Peptide Functionalized Titanium Surfaces

Enzymatic stability was a critical determinant for the functional longevity of antimicrobial surfaces in complex physiological environments. Theoretically, peptides composed entirely of D-amino acids should show superior resistance to proteolysis due to the strict chiral specificity of proteases. To validate this advantage on immobilized peptides, we treated the functionalized titanium surfaces with proteinase K and reassessed their antibacterial efficacy (Figure 3a). The results provided compelling quantitative support for the theory (Figure 3b,c). For the Ti-L-80 surface, proteinase K treatment caused an almost complete loss of function, where antibacterial rates dropped from 86.18% to 2.72% against *S. aureus* and from 90.59% to 4.40% against *E. coli*. This abrupt inactivation confirmed the high susceptibility of surface-tethered L-peptides to enzymatic degradation. In stark contrast, the Ti-D-80 surface showed remarkable stability. After identical protease treatment, it retained high antibacterial activity, with rates reaching 94.55% against *S. aureus* and 90.03% against *E. coli*. This pronounced functional preservation directly demonstrated that D-amino acid substitution effectively conferred protease resistance to surface-immobilized peptides, ensuring their antibacterial potency in enzyme-rich environments.

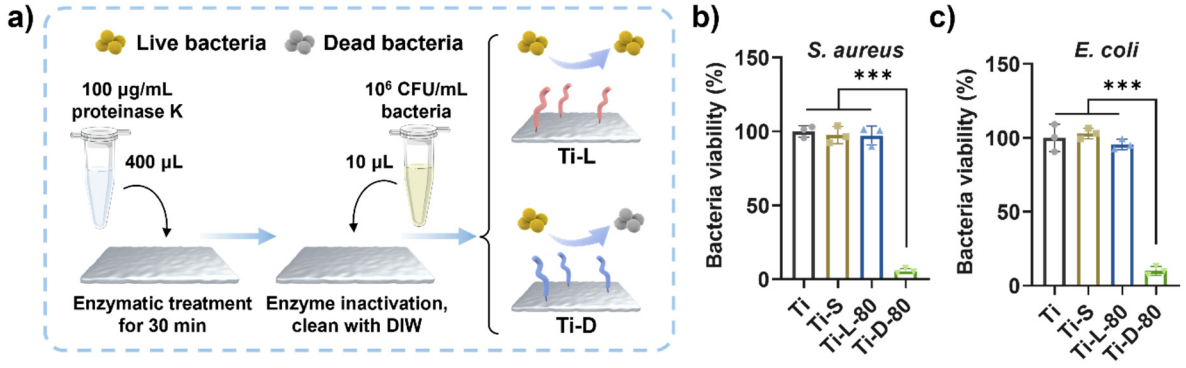

Figure 3. Enzymatic stability of peptide-functionalized titanium surfaces. (**a**) Schematic diagram of the enzymatic stability experiment. Antibacterial efficacy of surfaces following proteinase K treatment against (**b**) *S. aureus* and (**c**) *E. coli* (n = 3). *** denoted $p < 0.001$.

3.4. Biocompatibility of Peptide Functionalized Titanium Surfaces

The antibacterial results indicated that surfaces grafted with peptide concentrations below 40 μM lacked significant antibacterial activity (Figure 2b). Accordingly, only samples functionalized at 40, 50, and 80 μM were selected for biocompatibility assessment using L929 cells. CCK-8 results indicated a clear dependence of cellular response on both peptide type and surface density (Figure 4a–c). For Ti-L surfaces, increasing the grafting density from 40 to 80 μM progressively reduced biocompatibility. Specifically, on days 1, 3, and 5, compared with Ti, the CCK-8 OD values for Ti-L-80 decreased by 27.54%, 7.01%, and 7.21%, respectively (Figure 4a–c). The number of cells on Ti-L-80 was also visibly lower than on Ti (Figure 4d). In contrast, Ti-D surfaces exhibited biocompatibility comparable to Ti. Relative to Ti, on days 1, 3, and 5, the CCK-8 OD values for Ti-D-80 were

1.11-, 1.08-, and 1.04-fold, respectively (Figure 4a–c). Ti-D also demonstrated improved biocompatibility compared to Ti-L. For example, compared to Ti-L-80, the CCK-8 OD values for Ti-D-80 on days 1, 3, and 5 were 1.53-, 1.16-, and 1.12-fold, respectively (Figure 4a–c). Furthermore, cell morphology observations from day 1 to day 5 revealed that Ti-D surfaces supported more cells than Ti-L surfaces. Even at the highest grafting density (80 μM), cells on Ti-D maintained favorable morphology and adhesion, with no significant reduction in cell number or proliferation compared to Ti, confirming the excellent biocompatibility of Ti-D across all tested conditions (Figure 4d).

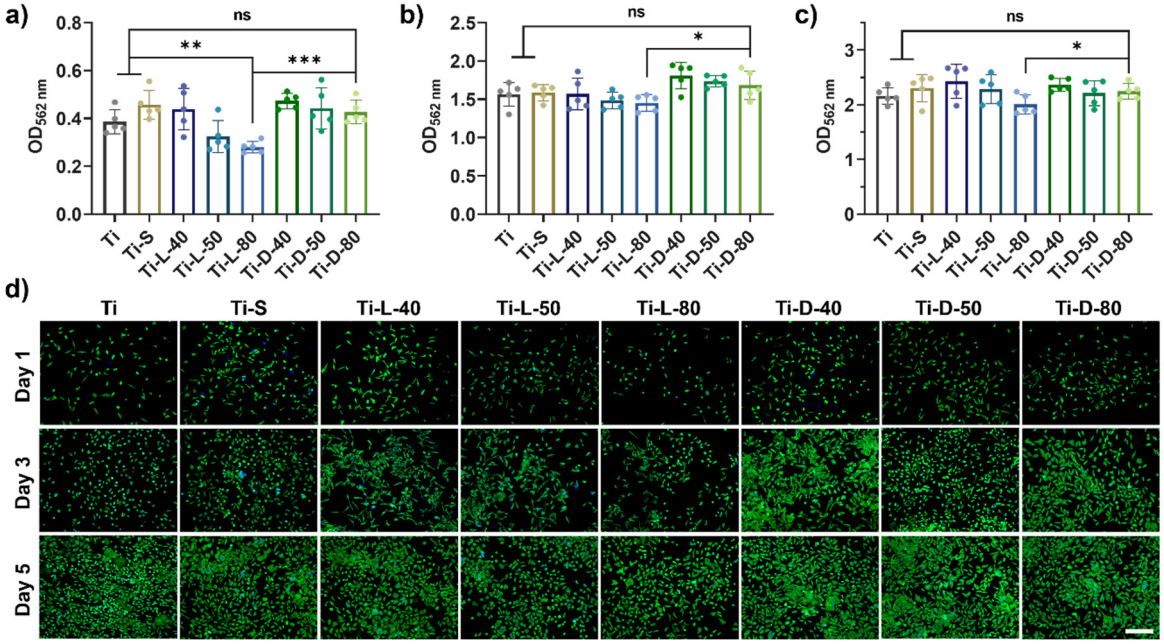

Figure 4. Biocompatibility of peptide functionalized titanium surfaces. Viability of L929 cells co-cultured with the indicated surfaces assessed by CCK-8 assay after (**a**) 1 day, (**b**) 3 days, and (**c**) 5 days of culture (n = 5). (**d**) Corresponding cell morphology images. Cells were stained with Phalloidin-FITC and DAPI and observed by fluorescence microscope (scale bar = 250 μm). * Denoted $p < 0.05$, ** denoted $p < 0.01$, *** denoted $p < 0.001$.

Together, these findings demonstrated that complete substitution with D-amino acids effectively reduced the cytotoxicity associated with high densities of L-peptide, thereby substantially enhancing the overall biocompatibility of the functionalized surface.

4. Discussion

This study compared the antibacterial performance and biocompatibility of L-peptides and their fully D-substituted counterparts (D-peptides), both in free solution and after surface grafting. The results showed that complete D-amino acid substitution markedly enhanced the antibacterial activity of the original L-peptide against both *S. aureus* and *E. coli*, whether in solution (Figure 2a) or after surface grafting (Figure 2b). Consistent with previous reports, the effect of D-substitution on antibacterial activity depended on the mechanism of the antimicrobial peptide. D-substitution generally maintained the activity of peptides that act via nonspecific membrane disruption, such as KWKKLLKKPLLKKLLKKL [30], KKLLKLLKLLL [31], and FLPLIGRVLSGIL [32], whereas it often reduced the activity of peptides that rely on stereospecific target binding, exemplified by Bac(1–17) [33]. It was also worth noting that selective D-substitution at individual residues can further modulate antibacterial activity by altering peptide conformation [34]. Furthermore, our results demonstrated that D-substitution did not compromise the bacterial membrane-disruptive mechanism of the peptide (Figure 2d), thereby retaining its ability to evade conventional resistance mechanisms.

In addition to its influence on antibacterial performance, D-substitution significantly improved proteolytic stability (Figure 3). This characteristic was critical for extending functional durability under physiological conditions and represents a key factor in enhancing the therapeutic potential of peptide-based coatings [35,36]. For bone-titanium implants, long-term in vivo stability of antimicrobial coatings is essential to clinical translation [6,37]. Without sufficient resistance to endogenous proteases, surface coatings degrade rapidly, resulting in transient antibacterial activity that permits biofilm formation and infection recurrence [38]. The use of D-amino acids directly addresses

this limitation by conferring pronounced protease resistance, thereby aligning peptide durability with the long-term functional demands of orthopedic implants [39,40].

For antimicrobial peptide-functionalized surfaces, achieving favorable biocompatibility remained a major challenge due to the high local density of peptides. Our results showed that L-peptide-functionalized surfaces (Ti-L) indeed exhibited certain cytotoxicity (Figure 4), which may hinder tissue regeneration. In contrast, D-substituted antimicrobial peptides in this work demonstrated excellent biocompatibility (Figure 4). The Ti-D-80 surface supported a cell density comparable to that on the pristine Ti control, which was significantly higher than that on the Ti-L-80 surface. According to previous reports, this improvement could be attributed to the ability of D-substitution to modulate peptide helicity and amphipathicity, thereby reducing toxicity [34,41]. Additionally, the mirror-image conformation of D-peptides helped them evade stereospecific recognition by eukaryotic cellular systems, avoiding bio-derived toxicity [42,43]. Nevertheless, the precise molecular mechanisms underlying these effects required further investigation.

Collectively, by simultaneously enhancing antibacterial efficacy, improving resistance to enzymatic degradation, and promoting biocompatibility, D-substitution broadens the therapeutic window of antibacterial surfaces. This integrated approach offers a promising design strategy for implant coatings that effectively balance strong antibacterial protection with favorable host tissue compatibility.

5. Conclusions

The surface immobilization of D-amino acid-substituted antimicrobial peptides onto titanium implants produced interfaces with significantly improved performance. Compared with conventional L-peptide coatings, the Ti-D surface not only exhibited potent broad-spectrum antibacterial activity through a membrane-disruptive mechanism and demonstrated strong resistance to enzymatic degradation, but also maintained excellent biocompatibility even at high grafting densities. Together, these properties established D-amino acid substitution as an effective molecular strategy for designing implant surfaces that combined robust, long-lasting antibacterial protection with enhanced compatibility toward host tissues, thereby advancing the development of infection-resistant biomedical interfaces.

Author Contributions

R.Z.: investigation, methodology, data curation, visualization, writing—original draft preparation; L.W.: conceptualization, methodology, funding acquisition, writing—reviewing and editing, funding acquisition; Y.W.: supervision, conceptualization, funding acquisition.

Funding

This work was financially supported by the National Key R&D Program of China (2023YFB3809901), the National Natural Science Foundation of China (Grant No. 52571269), Science and Technology Program of Guangzhou (SL2023A04J00808).

Institutional Review Board Statement

Not applicable. This study did not involve human participants or animal experiments.

Informed Consent Statement

Not applicable.

Data Availability Statement

The data in this study are available from the corresponding author on reasonable request.

Conflicts of Interest

The authors declare no conflict of interest. Given the role as Editorial Board Member, Lin Wang had no involvement in the peer review of this paper and had no access to information regarding its peer-review process. Full responsibility for the editorial process of this paper was delegated to another editor of the journal.

Use of AI and AI-Assisted Technologies

During the preparation of this work, the authors used ChatGPT to polish the language. After using this tool, the authors reviewed and edited the content as needed and take full responsibility for the content of the published article.

References

1. Geetha, M.; Singh, A.K.; Asokamani, R.; et al. Ti based biomaterials, the ultimate choice for orthopaedic implants—A review. *Prog. Mater. Sci.* **2009**, *54*, 397–425. https://doi.org/10.1016/j.pmatsci.2008.06.004.
2. Moriarty, T.F.; Metsemakers, W.-J.; Morgenstern, M.; et al. Fracture-related infection. Nature Reviews Disease Primers **2022**, *8*, 67. https://doi.org/10.1038/s41572-022-00396-0.
3. Bozic, K.J.; Kurtz, S.M.; Lau, E.; et al. The Epidemiology of Revision Total Knee Arthroplasty in the United States. *Clin. Orthop. Relat. Res.* **2010**, *468*, 45. https://doi.org/10.1007/s11999-009-0945-0.
4. Stewart, P.S.; William Costerton, J. Antibiotic resistance of bacteria in biofilms. *Lancet* **2001**, *358*, 135–138. https://doi.org/10.1016/S0140-6736(01)05321-1.
5. Davies, D. Understanding biofilm resistance to antibacterial agents. *Nat. Rev. Drug Discov.* **2003**, *2*, 114–122. https://doi.org/10.1038/nrd1008.
6. Kargupta, R.; Bok, S.; Darr, C.M.; et al. Coatings and surface modifications imparting antimicrobial activity to orthopedic implants. *Wiley Interdiscip. Rev.-Nanomed. Nanobiotechnol.* **2014**, *6*, 475–495. https://doi.org/10.1021/10.1002/wnan.1273.
7. Lange, J.; Troelsen, A.; Thomsen, R.W.; et al. Chronic infections in hip arthroplasties: Comparing risk of reinfection following one-stage and two-stage revision: A systematic review and meta-analysis. *Clin. Epidemiol.* **2012**, *4*, 57–73. https://doi.org/10.2147/CLEP.S29025.
8. Masters, E.A.; Trombetta, R.P.; de Mesy Bentley, K.L.; et al. Evolving concepts in bone infection: Redefining "biofilm", "acute vs. chronic osteomyelitis", "the immune proteome" and "local antibiotic therapy". *Bone Res.* **2019**, *7*, 20. https://doi.org/10.1038/s41413-019-0061-z.
9. Yılmaz, Ç.; Özcengiz, G. Antibiotics: Pharmacokinetics, toxicity, resistance and multidrug efflux pumps. *Biochem. Pharmacol.* **2017**, *133*, 43–62. https://doi.org/10.1016/j.bcp.2016.10.005.
10. Zhang, H.; Chen, Q.; Xie, J.; et al. Switching from membrane disrupting to membrane crossing, an effective strategy in designing antibacterial polypeptide. *Sci. Adv.* **2023**, *9*, eabn0771. https://doi.org/10.1126/sciadv.abn0771.
11. Li, J.; Tan, L.; Liu, X.; et al. Balancing Bacteria–Osteoblast Competition through Selective Physical Puncture and Biofunctionalization of ZnO/Polydopamine/Arginine-Glycine-Aspartic Acid-Cysteine Nanorods. *ACS Nano* **2017**, *11*, 11250–11263. https://doi.org/10.1021/acsnano.7b05620.
12. Zhao, F.; Gao, A.; Liao, Q.; et al. Balancing the Anti-Bacterial and Pro-Osteogenic Properties of Ti-Based Implants by Partial Conversion of ZnO Nanorods into Hybrid Zinc Phosphate Nanostructures. *Adv. Funct. Mater.* **2024**, *34*, 2311812. https://doi.org/10.1002/adfm.202311812.
13. Standert, V.; Borcherding, K.; Bormann, N.; et al. Antibiotic-loaded amphora-shaped pores on a titanium implant surface enhance osteointegration and prevent infections. *Bioact. Mater.* **2021**, *6*, 2331–2345. https://doi.org/10.1016/j.bioactmat.2021.01.012.
14. Wang, K.; Rong, F.; Peng, H.; et al. Infection Microenvironment-Responsive Coating on Titanium Surfaces for On-Demand Release of Therapeutic Gas and Antibiotic. *Adv. Healthc. Mater.* **2024**, *13*, 2304510. https://doi.org/10.1002/adhm.202304510.
15. Wang, K.; Gao, M.; Fan, J.; et al. $SrTiO_3$ Nanotube-Based "Pneumatic Nanocannon" for On-Demand Delivery of Antibacterial and Sustained Osseointegration Enhancement. *ACS Nano* **2024**, *18*, 16011–16026. https://doi.org/10.1021/acsnano.4c04478.
16. Brogden, K.A. Antimicrobial peptides: Pore formers or metabolic inhibitors in bacteria? *Nat. Rev. Microbiol.* **2005**, *3*, 238–250. https://doi.org/10.1038/nrmicro1098.
17. Wang, J.; Dou, X.; Song, J.; et al. Antimicrobial peptides: Promising alternatives in the post feeding antibiotic era. *Med. Res. Rev.* **2019**, *39*, 831–859. https://doi.org/10.1002/med.21542.
18. Oliveira Júnior, N.G.; Souza, C.M.; Buccini, D.F.; et al. Antimicrobial peptides: Structure, functions and translational applications. *Nat. Rev. Microbiol.* **2025**, *23*, 687–700. https://doi.org/10.1038/s41579-025-01200-y.
19. Chen, R.; Willcox, M.D.P.; Ho, K.K.K.; et al. Antimicrobial peptide melimine coating for titanium and its in vivo antibacterial activity in rodent subcutaneous infection models. *Biomaterials* **2016**, *85*, 142–151. https://doi.org/10.1016/j.biomaterials.2016.01.063.
20. Dong, J.; Chen, F.; Yao, Y.; et al. Bioactive mesoporous silica nanoparticle-functionalized titanium implants with controllable antimicrobial peptide release potentiate the regulation of inflammation and osseointegration. *Biomaterials* **2024**, *305*, 122465. https://doi.org/10.1016/j.biomaterials.2023.122465.
21. Li, M.; Bai, J.; Tao, H.; et al. Rational integration of defense and repair synergy on PEEK osteoimplants via biomimetic peptide clicking strategy. *Bioact. Mater.* **2022**, *8*, 309–324. https://doi.org/10.1016/j.bioactmat.2021.07.002.
22. He, X.; Zhang, J.; Xie, L.; et al. Phytic Acid-Promoted rapid fabrication of natural polypeptide coatings for

multifunctional applications. *Chem. Eng. J.* **2022**, *440*, 135917. https://doi.org/10.1016/j.cej.2022.135917.

23. Mohamed, M.F.; Brezden, A.; Mohammad, H.; et al. A short D-enantiomeric antimicrobial peptide with potent immunomodulatory and antibiofilm activity against multidrug-resistant Pseudomonas aeruginosa and Acinetobacter baumannii. *Sci. Rep.* **2017**, *7*, 6953. https://doi.org/10.1038/s41598-017-07440-0.
24. Hamamoto, K.; Kida, Y.; Zhang, Y.; et al. Antimicrobial Activity and Stability to Proteolysis of Small Linear Cationic Peptides with D-Amino Acid Substitutions. *Microbiol. Immunol.* **2002**, *46*, 741–749. https://doi.org/10.1111/j.1348-0421.2002.tb02759.x.
25. McGrath, D.M.; Barbu, E.M.; Driessen, W.H.P.; et al. Mechanism of action and initial evaluation of a membrane active all-D-enantiomer antimicrobial peptidomimetic. *Proc. Natl. Acad. Sci. USA* **2013**, *110*, 3477–3482. https://doi.org/10.1073/pnas.1221924110.
26. Lou, T.; Bai, X.; He, X.; et al. Antifouling performance of d-enantiomers-based peptide-modified aluminum alloy surfaces with enhanced stability against proteolytic degradation. *J. Mater. Sci.* **2023**, *58*, 15499–15512. https://doi.org/10.1007/s10853-023-08960-z.
27. Shi, G.; Kang, X.; Dong, F.; et al. DRAMP 3.0: An enhanced comprehensive data repository of antimicrobial peptides. *Nucleic Acids Res.* **2022**, *50*, D488-D496. https://doi.org/10.1093/nar/gkab651.
28. Kim, S.-J.; Kim, J.-S.; Lee, Y.-S.; et al. Structural Characterization of de Novo Designed L5K5W Model Peptide Isomers with Potent Antimicrobial and Varied Hemolytic Activities. *Molecules* **2013**, *18*, 859–876. https://doi.org/10.3390/molecules18010859.
29. Fu, J.; Zhu, W.; Liu, X.; et al. Self-activating anti-infection implant. *Nat. Commun.* **2021**, *12*, 6907. https://doi.org/10.1038/s41467-021-27217-4.
30. Park, S.-C.; Kim, J.-Y.; Lee, J.-K.; et al. Synthetic diastereomeric-antimicrobial peptide: Antibacterial activity against multiple drug resistant clinical isolates. *Pept. Sci.* **2011**, *96*, 130–136. https://doi.org/10.1002/bip.21446.
31. Personne, H.; Paschoud, T.; Fulgencio, S.; et al. To Fold or Not to Fold: Diastereomeric Optimization of an α-Helical Antimicrobial Peptide. *J. Med. Chem.* **2023**, *66*, 7570–7583. https://doi.org/10.1021/acs.jmedchem.3c00460.
32. Wade, D.; Silberring, J.; Soliymani, R.; et al. Antibacterial activities of temporin A analogs. *FEBS Lett.* **2000**, *479*, 6–9. https://doi.org/10.1016/S0014-5793(00)01754-3.
33. Loffredo, M.R.; Savini, F.; Bobone, S.; et al. Inoculum effect of antimicrobial peptides. *Proc. Natl. Acad. Sci. USA* **2021**, *118*, e2014364118. https://doi.org/10.1073/pnas.2014364118.
34. Huang, Y.; He, L.; Li, G.; et al. Role of helicity of α-helical antimicrobial peptides to improve specificity. *Protein Cell* **2014**, *5*, 631–642. https://doi.org/10.1007/s13238-014-0061-0.
35. Chen, H.-L.; Su, P.-Y.; Shih, C. Improvement of in vivo antimicrobial activity of HBcARD peptides by D-arginine replacement. *Appl. Microbiol. Biotechnol.* **2016**, *100*, 9125–9132. https://doi.org/10.1007/s00253-016-7621-6.
36. Ng, S.M.S.; Teo, S.W.; Yong, Y.E.; et al. Preliminary investigations into developing all-D Omiganan for treating Mupirocin-resistant MRSA skin infections. *Chem. Biol. Drug Des.* **2017**, *90*, 1155–1160. https://doi.org/10.1111/cbdd.13035.
37. Liu, M.; Svirskis, D.; Proft, T.; et al. Progress in peptide and protein therapeutics: Challenges and strategies. *Acta Pharm. Sin. B* **2025**, *15*, 6342–6381. https://doi.org/10.1016/j.apsb.2025.10.026.
38. Gellert, M.; Hardt, S.; Köder, K.; et al. Biofilm-active antibiotic treatment improves the outcome of knee periprosthetic joint infection: Results from a 6-year prospective cohort study. *Int. J. Antimicrob. Agents* **2020**, *55*, 105904. https://doi.org/10.1016/j.ijantimicag.2020.105904.
39. Caldwell, M.; Hughes, M.; Wei, F.; et al. Promising applications of D-amino acids in periprosthetic joint infection. *Bone Res.* **2023**, *11*, 14. https://doi.org/10.1038/s41413-023-00254-z.
40. Duan, S.; Wu, R.; Xiong, Y.-H.; et al. Multifunctional antimicrobial materials: From rational design to biomedical applications. *Prog. Mater. Sci.* **2022**, *125*, 100887. https://doi.org/10.1016/j.pmatsci.2021.100887.
41. Oren, Z.; Shai, Y. Selective Lysis of Bacteria but Not Mammalian Cells by Diastereomers of Melittin: Structure−Function Study. *Biochemistry* **1997**, *36*, 1826–1835. https://doi.org/10.1021/bi962507l.
42. Arranz-Gibert, P.; Ciudad, S.; Seco, J.; et al. Immunosilencing peptides by stereochemical inversion and sequence reversal: Retro-D-peptides. *Sci. Rep.* **2018**, *8*, 6446. https://doi.org/10.1038/s41598-018-24517-6.
43. Yang, J.; Ran, Y.; Liu, S.; et al. Synergistic D-Amino Acids Based Antimicrobial Cocktails Formulated via High-Throughput Screening and Machine Learning. *Adv. Sci.* **2024**, *11*, 2307173. https://doi.org/10.1002/advs.202307173.